

Article

Isolation, Characterization, and Anti-idiopathic Pulmonary Fibrosis Activity of a Fucoidan from *Costaria costata*

Sijie Wei ^{1,3}, Lihua Geng ¹, Haoyu Yu ^{1,3}, Jing Wang ¹, Yang Yue ¹, Quanbin Zhang ^{1,3} and Ning Wu ^{1,2,4,*}

¹ CAS and Shandong Province Key Laboratory of Experimental Marine Biology, Center for Ocean Mega-Science, Institute of Oceanology, Chinese Academy of Sciences, Qingdao, China

² Drugs and Bioproducts, Qingdao National Laboratory for Marine Science and Technology, Qingdao, China

³ University of Chinese Academy of Sciences, Beijing, China

⁴ Nantong Zhongke Marine Science and Technology Research and Development Center, Nantong, China

* Correspondence: wuning@qdio.ac.cn

Abstract: Pulmonary fibrosis is a chronic, progressive and fatal disease of the interstitial lung. There still lack of efficient therapy to reverse the prognosis of patients currently. In this study, a fucoidan from *Costaria costata* was isolated and its anti-idiopathic fibrosis activity was investigated both *in vitro* and *in vivo*. The chemical composition analysis results show that *C. costata* polysaccharide (CCP) is consisting of galactose and fucose as the main monosaccharides with a sulfate group content of 18.54%. Further study found that CCP could resist TGF- β 1-induced epithelial-mesenchymal transition (EMT) in A549 cells by inhibiting the TGF- β /Smad and PI3K/AKT/mTOR signaling pathways. Moreover, *In vivo* study found that CCP treatment alleviated bleomycin (BLM)-stimulated fibrosis and inflammation in mice lung tissue. In conclusion, the present study suggests that CCP could protect the lung from fibrosis by relieving the EMT process and inflammation in lung cells.

Keywords: *Costaria costata*; fucoidan; idiopathic pulmonary fibrosis

1. Introduction

Idiopathic pulmonary fibrosis (IPF) is characterized by diffuse interstitial fibrotic change in lung parenchymal [1]. Because of its rapid deterioration and high lethality, it is considered a difficult pulmonary disease by the World Health Organization [2]. The pathological symptom of IPF in the early stages is alveolar inflammation involving fibroblast proliferation and massive extracellular matrix (ECM) deposition. Eventually, this abnormal accumulation of collagen leads to pulmonary fibrosis. A number of signal pathways have been implicated in the pathogenesis of IPF. Among these, the TGF- β /Smad signal pathway plays an essential role.

The streamer kelp *C. costata* is in the order *Laminariales*, family *Costariaceae* [3], which is an annual plant found mainly in Troits Bay in the Sea of Japan and in Russia [4]. *C. costata* has an undivided blade over 30 centimeters in width and about 150 centimeters long, and grows to largest size in June [5], it has been used as edible seaweed for a long time in Japan and as a nutritious feedstuff for *Abalone*, *Haliotis*. In recent years, *C. costata* has been successfully introduced to the coast of Dalian in northern China for captive breeding.

Fucoidan is a water-soluble polysaccharides with a sizable quantity of fucose and sulfate groups. It is mainly derived from brown algae and is also found in marine invertebrates [6]. Kylin isolated fucoidan for the first time in 1913 and gave it the name "fucoidin" [7]. The structure and function of fucoidan varies according to the species of brown algae and extraction techniques. For instance, January evaluated three different fucoidan extraction techniques: hot water extraction, salt extraction, and acid extraction. It was found that hot water extraction provides maximum yield of fucoidan [8].

The fucoidan derived from *C. costata* has a wide range of biological activities, such as anti-hyperlipidemia [9], anti-skin photoaging [3], and anti-CCl₄-induced liver injury [4]. However, there are no relative research about the anti-idiopathic pulmonary fibrosis activity of fucoidan from *C. costata*, so in the present study we isolated fucoidan (CCP) from *C. costata* by hot water extraction method, analysed chemical composition of CCP and firstly evaluated its anti-idiopathic fibrosis activity both *in vitro* cell model and *in vivo* mice model.

2. Materials and Methods

2.1. Reagents and chemicals

Sulphuric acid (95~98%), sodium hydroxide (≥99.0%), hydrogen peroxide (30%), phenol (≥99.0%), ethanol (95%) and hydrochloric acid (12 M) were purchased from Sinopharm (Shanghai, China); RPMI medium was purchased from Hyclone (Logan, UT, USA); 1-phenyl-3-methyl-5-pyrazolone (PMP), 3-(4, 5-dimethylthiazol-2-yl)-2, 5-diphenyltetrazolium bromide (MTT) reagent, standards for monosaccharide composition analysis, dimethylsulfoxide (DMSO) and trifluoroacetic acid (TFA) were purchased from Sigma-Aldrich (St. Louis, MO, USA); Fetal bovine serum (FBS) was purchased from Biological Industries (Israel); Enzyme-linked immunosorbent assay (ELISA) kit of interleukin-6 (IL-6) production analysis was obtained from Mlbio (Shanghai, China); The total phenolic assay (TPA) kit was provided by Boxbio (Beijing, China) and the bicinchoninic acid assay (BCA) kit was provided by Solarbio (Beijing, China); Transforming growth factor beta 1 (TGF-β1) was provided by GenScript (Nanjing, China); TGF-β1 inhibitor SB431542 was obtained from Beyotime (Nantong, Jiangsu, China); Bleomycin (BLM) was obtained from Nippon Kayaku (Takasaki, Japan); Nintedanib (Nin) was purchased from Yuanye Bio-Technology (Shanghai, China); Griess reagent, Hypersensitive reaction and pathogenicity gene (HRP) conjugated goat anti-mouse immunoglobulin G (IgG) secondary antibodies and 4',6-diamidino-2-phenylindole (DAPI) were provided by Beyotime (Nantong, Jiangsu, China); HRP conjugated goat anti-rabbit IgG secondary antibodies and antibodies to phosphorylated Smad2/3 (p-Smad2/3), phosphorylated AKT (p-AKT), phosphorylated m-TOR (p-mTOR) were purchased from Affinity (Chicago, IL, USA); Antibodies to collagen II alpha 1 (COL2A1), AKT, mTOR, TGF-β1 were purchased from Santa Cruz (Dallas, TX, USA).

2.2. *Costaria costata* polysaccharides (CCP) extraction and analysis

2.2.1. CCP extraction

C. costata is purchased from Hokkaido, Japan in 2017. To isolate the crude CCP from *C. costata*, a hot water extraction method was utilized [10,11]. Briefly, the *C. costata* fragments were soaked in hot water at a ratio of 1:10, and heated in the autoclave for 120 minutes without stirring at 120°C at high pressure. After filtered residue out and condensed to 2 liters by spin evaporation, CaCl₂ was added to the concentrate with a final concentration of 0.2 M in order to produce the precipitated sodium alginate (SA), and the filtrate was dialyzed for 24 hours using a 12,000 Da dialysis bag. Then we poured the filtrate into three times volume of ethanol for alcohol precipitation and dried the resulting precipitate with high-temperature baking lamps to get crud CCP. Crude CCP was resolved into a 2% solution, then added 4% granular activated carbon (GAC), and this mixture was stirred at 50 °C for an hour to reduce the pigment. After this, the calcium ions and magnesium ions were removed using a cation exchange column to purify CCP. The yield rate of CCP was calculated by following formula (Eq. 1):

$$\text{Yield rate} = \frac{\text{Dry weight of CCP}}{\text{Dry weight of } \textit{Costaria costata}} \times 100\% \quad (1)$$

2.2.2. Chemical analysis

The glucuronide content of CCP was determined using the carbazole colorimetric method [12.] The total sugar content of CCP was assayed by the phenol-sulfuric acid colorimetric method [13] with fucose as the standard. The cysteine hydrochloride method was used to determine the fucose content [14]. The protein content of CCP was determined using the Bicinchoninic Acid (BCA) Assay kit (Beijing Solarbio Science & Technology Co., Ltd.). Using ion chromatography, CCP was eluted with 4.5 mmol/L Na₂CO₃ and 0.8 mmol/L NaHCO₃ mixture solution at a flow rate of 1.0 mL·min⁻¹ by IC SI-52 4E column (Dionex IonPac AS 23-4μm 4 mm) at 45 °C to determinate the sulfate group content.

2.2.3. Determination of CCP-Molecular weight

The mass-averaged molar mass of CCP was determined by the high-performance gel permeation chromatography-multiple angle laser light scattering (HPGPC-MALLS) method. CCP was eluted with 0.1 mol/L Na₂SO₄ using a TSK-Gel 3000PWXL (7.8 mm×300 mm) column from TOSOH, Japan, and then monitored at 40 °C using a refractive index detector. To plot the standard curve, eight dextrose (64650,36800,13150,9750,5250 and 2700 Da) were used as standards.

2.2.4. Monosaccharide determination

The monosaccharide composition of CCP was measured by the method of pre-column derivation reversed-phase high-performance liquid chromatography (RP-HPLC) [15]. CCP (5 mg/mL) was hydrolyzed by 2 mol/L trifluoroacetic acid (TFA) for 4 h at 110 °C and then neutralized using 2 mol/L NaOH. Samples or standards were added with ribose as internal standard, respectively, and reacted with 0.5 mol/L PMP for 30 min at 70 °C under alkaline conditions, then neutralized using hydrochloric acid after derivatization. The derivatives were extracted by chloroform and performed high-performance liquid chromatography (HPLC) analysis with the chromatographic condition in 40 °C, using a C18 reverse separation column (InertSustain, Japan, 4.6 mm×150 mm) and an SPD-20A UV-detector (Shimadzu, Kyoto, Japan) (245 nm), the flow rate was 1 mL/min, and the lysate consisted of 83% 0.1 M KH₂PO₄ buffer and 17% acetonitrile. To plot the standard curve, L-fucose (Fuc), D-galactose (Gal), D-mannose (Man), D-glucuronic acid (GlcA), L-rhamnose (Rha), D-glucose (Glc), D-ribose (Rib), D-xylose (Xyl) were used as standards. Then calculate each monosaccharide content by ratio of peak area to molecular weight of monosaccharides.

2.2.5. Attenuated Total Refraction-Fourier transform infrared (ATR-FTIR) spectroscopy

The functional groups of CCP were identified by ATR-FTIR using a Nicolet iS 10 FT-IR spectrometer (Thermo Fisher, Waltham, MA, USA) in the wave number range of 400 to 4000 cm⁻¹.

2.3. Cell culture and treatment

Human non-small cell lung cancer cells (A549 cells) were purchased from Shanghai Institute of Biological Sciences Resource Center, Chinese Academy of Sciences. A549 cells were cultured in RPMI 1640 medium supplemented with 10% FBS and 5% CO₂.

After cell apposition, TGF-β1 was added to all cell groups except the negative control group at a final concentration of 10 ng/mL, the SB431542 was added to the positive control group to make its final concentration 4 μM, and CCP (200 mg/mL) was added to the experimental group. After administration, the cells were incubated at 37 °C and 5% CO₂ for 36 h.

2.4. Animal models and drug treatment

Male C57BL/6J mice at 6-7 weeks age, were obtained from Viewsolid Biotech (Beijing, China). Animals were housed at 23 ± 2 °C with a 12 h dark/light cycle. All animals had free access to food and water and were humanely cared for throughout the study. All animals were cared for in accordance with the National Institute of Health Guide for the Care and Use of Laboratory Animals, and the Experimental Design of this study was approved by the Animal Experimentation Ethics Committee of the Institute of Oceanography, Chinese Academy of Sciences(CTEC-2022-02-01).

Forty-eight male mice were divided equally into four groups, namely (1) negative control group (Neg), (2) BLM group, (3) BLM+Nin (50 mg/Kg), and (4) BLM+CCP (200 mg/kg) group. In detail, 5 mg/kg bleomycin sulfate (S1214, Selleck, Japan) was injected into the trachea of the mice and the mice in the negative control group were injected with an equal amount of normal saline. One day after the BLM injection, the BLM+CCP and BLM+Nin groups were given CCP 200 mg/kg or Nin 50 mg/Kg once a day by orally, respectively. the BLM and negative control groups were given the same amount of saline. Mice in each group were sacrificed after being over-anesthetized on the 17th day after surgery.

2.5. Cellular morphology analysis

After treatment cell morphological changes in A549 cells were observed using an inverted microscope (OLYMPUS-CKX41), Before scanning electron microscopy analysis, cell samples were prepared by dehydration in an alcohol gradient, and then cells were observed under a scanning electron microscopy (Hitachi-S-3400N).

2.6. Cell cytotoxicity assay

Assessment of A549 cell viability using MTT. In detail, A549 cells were treated with trypsin and then inoculated into 96-well plates at a concentration of 1×10^4 cells/well and incubated at 37°C , 5% CO_2 . Cells were treated as 2.3 described, after 36 hours of incubation, 10 μL MTT dye was then dropped into each well, the plate was carefully vortexed and incubated at 37°C for 4 hours at a concentration of 5% CO_2 . The solution was then gently aspirated from the wells, 150 μL of DMSO was added to each well and the absorbance was read at 490 nm after 10 minutes of shaking at room temperature [16].

The following formula was used to calculate the percentage of cell viability (Eq. 2):

$$\text{cell viability} = \frac{\text{Mean OD of individual Test Group}}{\text{Mean OD of control Group}} \times 100\% \quad (2)$$

2.7. Cell Wound-healing assay

Cells were incubated in six-well plates for the cell wound healing assay. After **oppositon**, the cells were cut off with the top of the straw, the fragments were removed with a cleaning solution. Then cultured with a new medium of 1% FBS and administered as described in 2.3 incubated for 36 hours. Cell migration images were taken at 0 and 36 hours. By randomly measuring the length of the incision at the same location at two-time points, 0 h and 36 h. Incision length was used to quantify the healing index of the incision by Image J, determined as a percentage.

2.8. HE and Masson staining

Lung tissue sections were stained with hematoxylin-eosin (HE) and Masson (Servicebio, Wuhan, China) as a means of assessing the degree of pulmonary fibrosis in each group. To assess the extent of pulmonary fibrosis, stained paraffin sections were observed under a light microscope and 5 arbitrarily selected areas were photographed and recorded. Quantitative score analysis was performed using Image J and averaged.

2.9. Immunofluorescence staining

A549 was planted on glass and cultured *in vitro* for 36 h as mentioned above. It was cured with 4% formaldehyde for 15 minutes, washed with PBS for 3 times, and impregnated with 0.01% TritonX-100 for 5 minutes. The cell was then sealed with 1% bovine serum albumin for 60 min at room temperature, then the prepared cells were incubated with TGF- β 1, COL2A1, or p-Smad 2/3 diluted at 1:1000 at 4°C overnight. Subsequently, In the mild and dark part of the room, allospecific secondary antibodies (AlexaFluor594-AffiniPure sheep anti-rabbit, or FITC labeled sheep anti-mouse) were stained 1 hour later. The staining time of that DAPI method was 5 minutes, then cells were rinsed

with PBS three times after that [17]. Finally, an anti-fluorescence quencher (Sigma-Aldrich, St. Louis, Mo, USA) was added. A laser scanning confocal microscope (Zeiss, Jena, Germany) was used to collect the images.

2.10. Western blot analysis

Fresh mice lung tissues or A549 cells were obtained and added to RIPA lysis solution to break up the tissues/cells, then centrifuged at 12000 r/min for 5 minutes at 4°C. Then collected supernatant and measured the protein concentration using the BCA method, adjusted to the same concentration with PBS and then added Loading Buffer and heating at 100°C for 5 minutes. 20 µg of protein sample was separated by 10% sodium dodecyl sulfate polyacrylamide gel electrophoresis (SDS-PAGE) and transferred to polyvinylidene fluoride (PVDF) membrane, the PVDF membrane was cut into different strips according to molecular weight, then blocked with 5% skimmed milk powder for one hour. After that, β-actin, TGF-β1, COL2A1, AKT, p-AKT, mTOR, p-mTOR primary antibodies were added to the corresponding bands respectively, diluted with 5% skimmed milk powder, all at a concentration of 1: 1000, and incubated overnight at 4°C. Then washed three times with TBST, 10 minutes each time. Incubated for 2 hours on a shaker using a 5% skimmed milk powder solution containing horseradish peroxidase-labeled secondary antibody (1: 1000 dilution), washed three times for 10 minutes each using TBST; visualized using the ECL Advanced Western Blot Detection Kit and images captured using a gel imaging system (BIO-RAD, USA); quantitative analysis using Image J.

2.11. Statistical analyses

All the statistics are carried out using the GraphPad Prism Version 6.02 version of GraphPad Prism (GraphPad Software in the United States). In this study, the data were processed by one-way ANOVA and post-hoc Turkey. Statistical significance was determined when *p < 0.05, **p < 0.01 and ***p < 0.001.

3. Results and Discussion

3.1. Chemical properties of CCP

Ethanol precipitation is currently the most commonly used method to extract polysaccharides due to the fact that polysaccharides are soluble in water but insoluble in organic solvents such as alcohols. Specifically, ethanol is added to the extraction solution to reduce the dielectric constant of the extraction solution so that the polysaccharides can be precipitated by dehydration [18]. The main process of alcohol precipitation is divided into crushing, leaching and alcohol precipitation, among which crushing and leaching have a great influence on the yield, quality and economy of obtaining polysaccharides [19]. In addition to mechanical crushing, novel techniques have emerged for the extraction of fucoidan, including ultrasound, microwave, and enzyme-assisted extraction [20]. Hot water extraction, dilute acid extraction and dilute alkali extraction are the main leaching methods [10-11]. Therefore, as its convenience and economy, a combination of mechanical crushing, hot water extraction and ethanol precipitation was chosen by us. The extraction and purification process of CCP is shown in Figure 1. The yield of CCP was 6.90% by hot water extraction, CCP was decolorized using activated carbon, and the absorbance at 580 nm was measured before and after decolorization, the decolorization rate was calculated to be 82.86% by the following equation (Eq. 3):

$$\text{Decolorization rate} = \frac{A_{\text{Before decolorization}} - A_{\text{After decolorization}}}{A_{\text{Before decolorization}}} \times 100\% \quad (3)$$

Typically, before bioactivity tests, the polysaccharide mixture is subjected to one or more purification processes to further enrich the extracts with the polysaccharides of interest [21]. Therefore, CCP was treated with cation exchange column chromatography to remove Ca²⁺ and Mg²⁺. The Ca²⁺ and Mg²⁺ contents before and after ion exchange were detected using an elemental analyzer,

yielding calcium and magnesium ion removal rates of 99.2% and 95.5%, respectively, calculated using the following equation (Eq. 4):

$$\text{Ion removal rate} = \frac{C_{\text{Before}} - C_{\text{After}}}{C_{\text{Before}}} \times 100\% \quad (4)$$

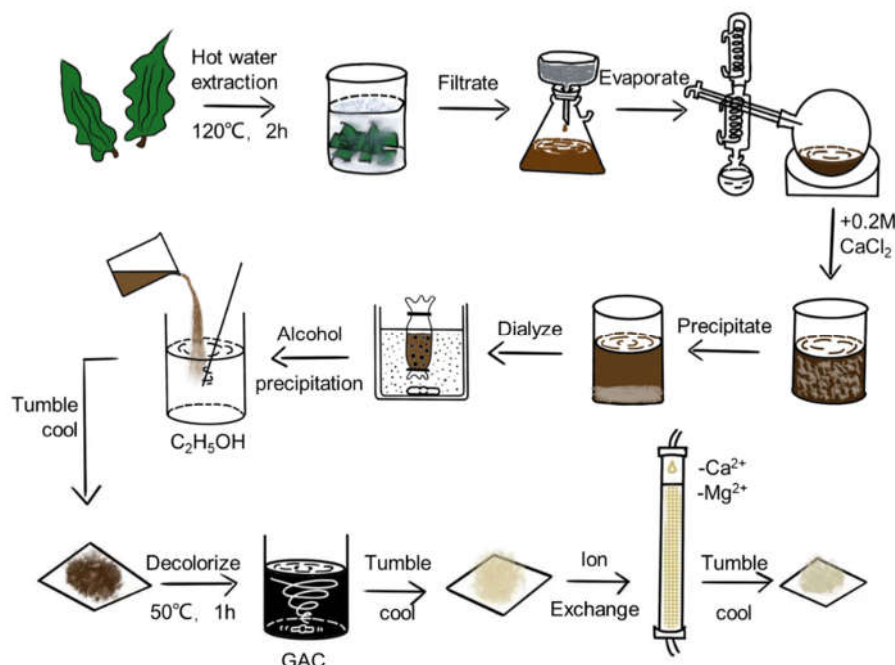


Figure 1. The extraction and purification process of CCP.

Proteins and phenolic compounds can also show some beneficial biological activity *in vitro* and *in vivo*, and they are usually mixed with polysaccharide together during polysaccharide extraction [22]. Prior to testing for biological activity, tests were carried out on the protein content and total phenolic content to exclude any effect they might have on the biological activity. The protein content of CCP was 1.38% by BCA, phenols were not detected in CCP. In addition, the sulfate group content was 18.54% by ion chromatography (Figure 2A and B) analysis. The total sugar content of CCP was 99.86% and the fucose content was 14.84% which using fucose as standard, the glucuronide content of CCP was 13.20% using glucuronide as standard, and the molecular weight of CCP was 149846 Da by HPLC (Table 1). The yield was calculated by Eq.1. Sulfate content, total sugar content, fucose content, GlcA content and protein content were calculated by standard curves respectively, which represent their content in CCP.

Table 1. CCP chemical composition analysis. (% , dry weight) and monosaccharide composition (molar ratio, Fuc=1).

Yield (%)	Sulfate content (%)	Fucose content (%)	GlcA content (%)	Protein content (%)	Molecular weight (Da)	Monosaccharide composition						
						Man	Rha	GlcA	Glc	Gal	Xyl	Fuc
6.90	18.54	14.85 ± 0.13	13.20 ± 0.26	1.38 ± 0.06	149846	0.244	0.111	0.073	0.042	0.906	0.03	1

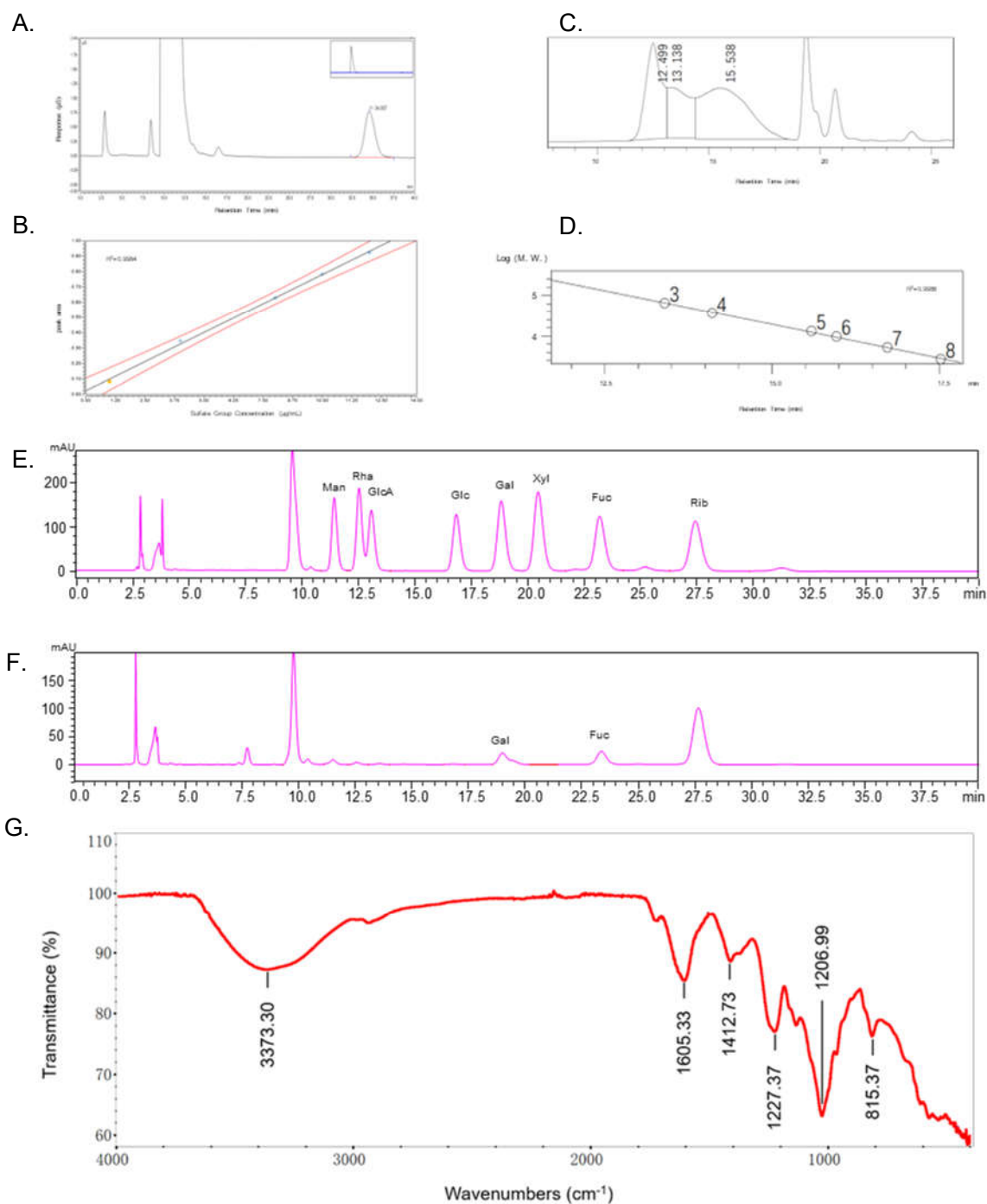


Figure 2. Chemical properties of CCP. (A) Determination of the sulfate group content of CCP by ion chromatography. (B) Standard curves for the determination of the sulfate group content (1 $\mu\text{g/mL}$, 2 $\mu\text{g/mL}$, 4 $\mu\text{g/mL}$, 6 $\mu\text{g/mL}$, 8 $\mu\text{g/mL}$, 10 $\mu\text{g/mL}$, 12 $\mu\text{g/mL}$). (C) Chromatogram for determination of the molecular weight of CCP. (D) Standard curve for molecular weight determination. (E) Chromatogram of standards for monosaccharide composition analysis (mannose (Man), rhamnose (Rha), glucuronide (GlcA), glucose (Glc), galactose (Gal), xylose (Xyl), fucose (Fuc)). (F) Chromatogram of CCP for monosaccharide composition analysis. (G) ATR-FTIR spectrum of CCP.

The molecular weight of CCP was calculated as 149.8 kDa according to the standard curve (Figure 2C and D). CCP mainly contains Fuc and Gal with a molar ratio of 1: 0.906, which indicated that CCP is a sulfated polymer of galactose and fucose (Figure 2E and F).

The infrared characteristics of CCP are shown in Figure 2G. There is a large, wide peak between 3100 and 3500 cm^{-1} , assigned as the vibration absorption of -OH. The variable angle vibration

absorption of the amide group N-H was at 1605 cm^{-1} . The variable angle vibration absorption of C-H were at 1412 cm^{-1} . The sharp and strong absorption peaks at about 1207 cm^{-1} and 1227 cm^{-1} was the S=O vibration absorption, there was characteristic absorption of sulfated or amino groups. In the fingerprint region, the sharp and weak peak at 815 cm^{-1} is classified as C-O-S stretching vibration absorption peak, suggesting that the sulfate substitution may be at the C-2 position [23]. The results showed CCP is an acidic polysaccharide.

3.2. CCP attenuated TGF- β 1-induced EMT in A549 cells

EMT is the terminal polarized epithelial to mesenchymal transition: injured epithelial cells transformed into fibroblasts and myofibroblasts, with the cells gaining migratory properties and losing the regeneration capacity of normal epithelial cells after transformation. TGF- β 1 is known to play a critical role in the EMT process. Several studies have used TGF- β 1 as an inducer for the transformation of polygonal epithelial cells into spindle-shaped fibrocytes [24]. In our study, A549 cells were induced using 10 ng/mL TGF- β 1 and administered with CCP ($200\mu\text{g/mL}$) or SB431542 ($4\mu\text{M}$), followed by 36 h of incubation. After this treatment, A549 cells were subjected to cytotoxicity assay using MTT. The results of our previous study showed that there was no significant change in cell survival in TGF- β 1, TGF- β 1+SB431542 and TGF- β 1 + CCP treated groups (Figure 3A). Compared with the blank control group, the cell viability of TGF- β 1 induction group, TGF- β 1+SB431542 group and TGF- β 1+CCP induction group decreased by 5.24%, 2.37% and 3.64%, respectively.

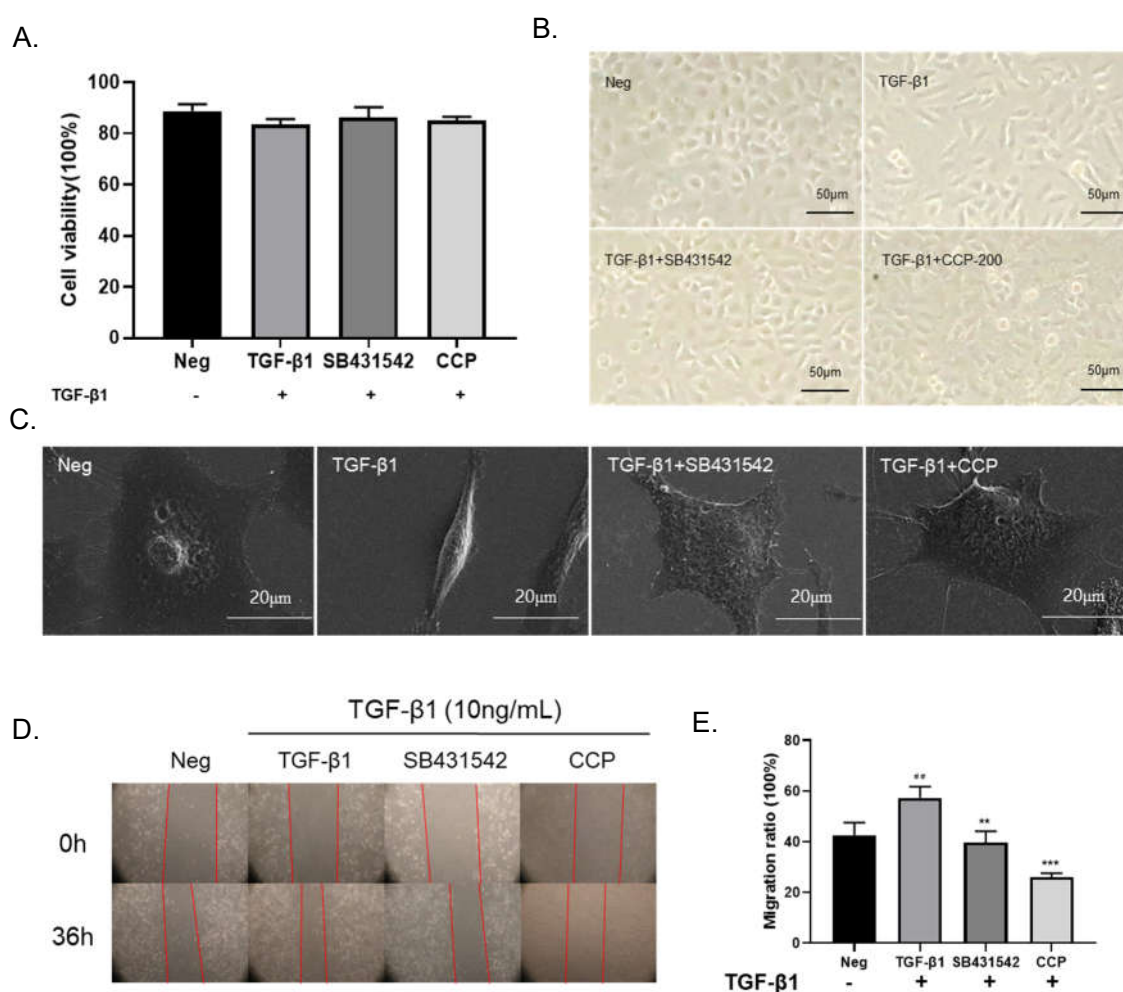


Figure 3. CCP attenuated TGF- β 1-induced EMT-like phenotypic change in A549 cells. Cell cytotoxic assay (A). TGF- β 1 (10 ng/mL), SB431542 ($4\text{ }\mu\text{M}$), CCP ($200\text{ }\mu\text{g/mL}$) Observation of cell morphology under an ordinary light microscope (B) and scanning electron microscope (C), Migration of A549 cells in the Neg, TGF- β 1, SB431542, and CCP groups when A549 cells were treated for 0 h and 36 h,

respectively. Images were taken with a 4× objective (D). Analysis of migration rate (%) compared to TGF-β1 group (E): **p < 0.01, ***p < 0.001, compared to control (Neg): ##p < 0.01. All values are mean ± standard error and were pooled from five independent experiments.

As Figure 3B shown, the morphology of the TGF-β1-induced cells changed to a narrow spindle shape with reduced intercellular contacts compared to the normal morphology of the negative control A549 cells, which were epithelial-like and polygonal. In terms of cell morphology, TGF-β1-induced not only changed cell morphology from the normal epithelial-like polygonal shape to the typical narrow shuttle shape but also reduced intercellular contacts. However, compared to the TGF-β1-induced group, 4 μM SB431542 or 200 μg/mL CCP treatment of cells restored intercellular contacts to normal polygonal shape and reproduced intercellular contacts [25]. We performed transmission electron microscopy (Figure 3C) to further validate the ameliorative effect of CCP on TGF-β1-induced EMT phenotypic alterations. The results revealed after the treatment of TGF-β1, the tumor tissue of A549 changed from the original prism to a long fusiform. However, the cell morphology resumed diamond shape in SB431542 and CCP-treated cells. These images illustrated that CCP attenuates TGF-β1-induced EMT-like phenotypic changes in A549 cells.

Growing evidences suggest that EMT causes significant morphological changes in differentiated epithelial cells and enhances their motility and invasive ability [26-27]. TGF-β1 induces cell migration and cell dedifferentiation, and it also regulates the expression of ECM components, such as fibronectin, elastin and collagen [28]. In order to investigate whether CCP has the ability to inhibit EMT, the migration and invasion ability of cells was assessed by wound-healing assay (Figure 3D and E). The results indicated that cell migration was dramatically increased in TGF-β1 induced cells compared with A549 cells, and SB431542 or CCP treatments were able to inhibit the enhanced migration ability of EMT to varying degrees. We demonstrated that CCP is able to inhibit TGF-β1-induced EMT in A549 cells from the perspective of cell migration.

3.3. CCP attenuates EMT by inhibiting both TGF-β/Smad and PI3K/AKT/mTOR signaling pathway

Generally speaking, the TGF-β1-induced EMT pathway can be divided into two types, Smad-dependent and Smad-independent paths, of which TGF-β1/Smad signal path is the most studied. [29-30]. TGF-β1 can interact with TGF-β receptors I and II (TGFβRI and TGFβRII) to promote the phosphorylation of Smad2/3 [31]. Phosphate-modified Smad2 and/or Smad3 bind to Smad4, then transport the conjugate into the cell and regulate EMT-related transcriptional molecules, such as Snail1, Twist1 and Slug [32-33]. In addition, non-Smad pathways have also been involved in the development of EMT [34]. For example, activation of the AKT pathway has important implications for TGF-β1-dependent EMT: in Wu's study [35], TGF-β1 can activate PI3K/AKT/mTOR and up-regulate the expression of COL2A1. Our findings are consistent with this. Using immunofluorescence, we found that TGF-β1 induction significantly increased the expression levels of TGF-β1, p-Smad 2/3 and COL2A1 in A549 cells, while SB431542 or CCP treatment decreased the expression of these cytokines (Figure 4A). It is suggested that CCP may promote the occurrence of EMT in lung cancer through TGF-β/Smad and its downstream molecular mechanism.

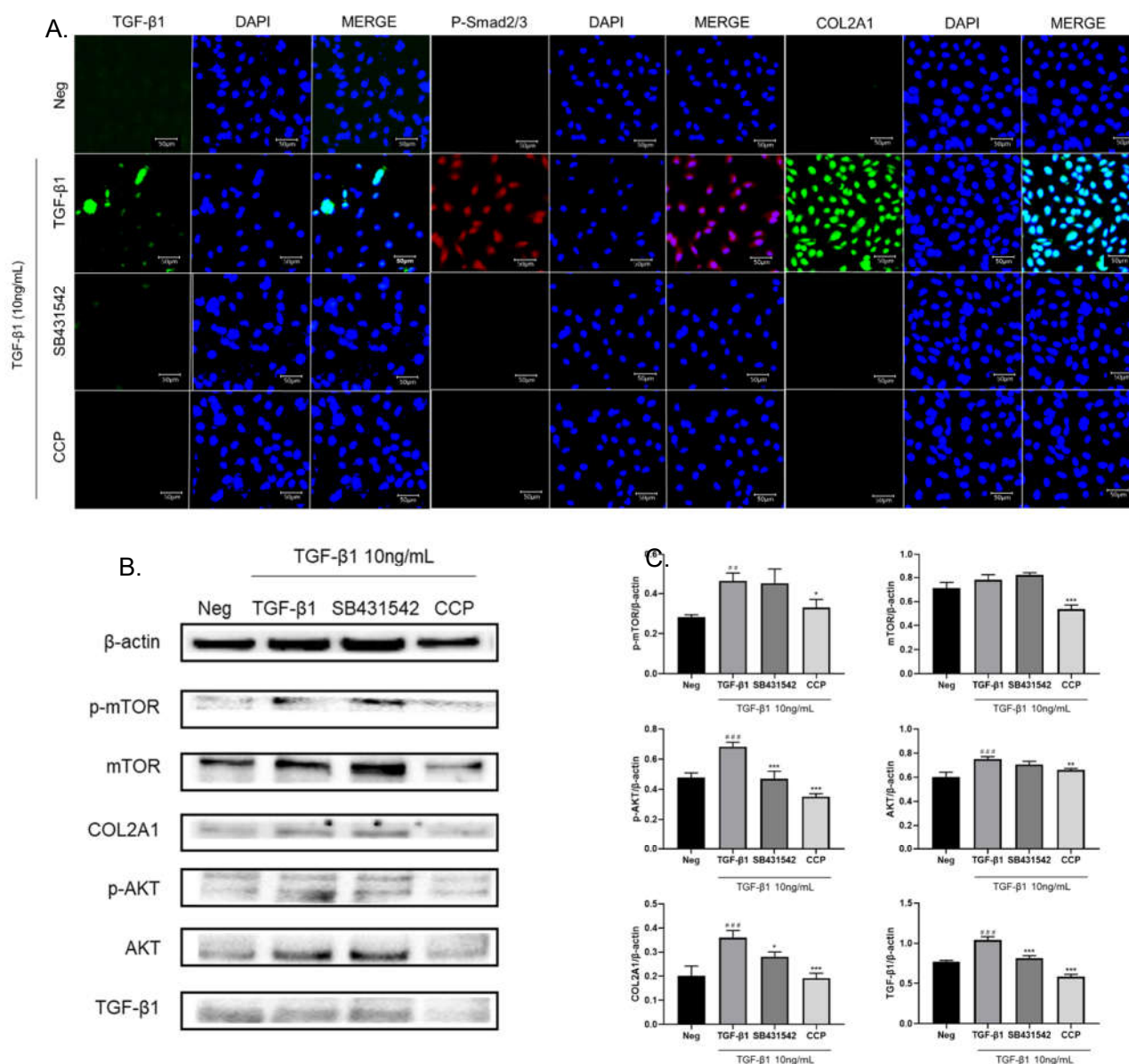


Figure 4. CCP impaired the TGF-β1-induced EMT process in A549 cells by inhibiting both TGF-β/Smad and PI3K/AKT/mTOR signaling pathway. (A) The protein levels of TGF-β1, p-Smad2/3 and COL2A1 from A549 cells treated with TGF-β1 (10 ng/mL), TGF-β1 plus SB431542 (4 μM), TGF-β1 plus CCP (200 μg/mL) or negative control (Neg) were determined by immunofluorescence, with scale lengths representing 50 μm. All values are mean ± standard error and were pooled from three independent experiments. (B) The protein levels of p-mTOR, mTOR, COL2A1, p-AKT, AKT and TGF-β1 from A549 cells treated with TGF-β1 (10 ng/mL), TGF-β1 plus SB431542 (4 μM), TGF-β1 plus CCP (200 μg/mL) or negative control (Neg) were determined by western blot, and analyzed by Image J (C), compared to TGF-β1 group. *p < 0.05, **p < 0.01, ***p < 0.001, compared to control (Neg); ##p < 0.01, ###p < 0.001.

As shown in Figure 4B and C, TGF-β1 induction significantly upregulated the expression of TGF-β1, COL2A1, mTOR, p-mTOR, AKT, and p-AKT. CCP administration significantly inhibited the elevated protein expression caused by TGF-β1, while the reduction effect of SB431542 administration was not statistically significant mentions to p-mTOR, mTOR and AKT. This result is consistent with the results of immunofluorescence, indicating that CCP alleviates the TGF-β1-induced EMT phenomenon in A549 cells by inhibiting the PI3K/AKT/mTOR pathway, and the TGF-β1/Smad pathway.

3.4. CCP attenuated lung EMT phenotype in a BLM-induced mice model

Intratracheal instillation of bleomycin (BLM) for rapid induction of pulmonary fibrosis (PF) is the classic method for establishing a well-defined PF mouse model. [36-37], and we established a fibrosis model in this way. The mice decreased in weight between 1-13 days post-operatively, with the BLM-induced mice declining the most weight and the CCP-induced mice declining the least. The weight of all groups except the CCP group ceased to drop after day 13. In the control group, the weight remained at normal levels. This suggests that the surgery caused a degree of weight loss in the mice, which was mitigated by CCP treatment. In terms of survival, the negative group (Neg) without any treatment had a 100% survival rate, the BLM-induced mice (BLM) had the lowest survival rate, the Nin-administration group (BLM+Nin) had the next lowest survival rate, and the CCP-treated mice had the highest survival rate among the different groups of surgically treated mice (Figure 5B). In addition, we also calculated the lung-to-weight ratio of mice after dissection. We found that due to the inflammatory response and fluid infiltration in the lungs, BLM induction caused a significant increase in the lung-to-weight ratio of mice compared to Neg group, while the Nin and CCP treatment groups decreased the weight of lungs (Figure 5C).

Overexpression of TGF- β 1 in the lung tissue of IPF patients is often an important feature. We examined the level of TGF- β 1 in the alveolar lavage fluid of mice by ELISA (Figure 5D) and found that the expression of TGF- β 1 was increased in BLM-induced mice and a reduced in Nin and CCP-treated mice compared with the BLM group, and the expression of TGF- β 1 in serum showed similar results (Figure 5E). The development of IPF is often accompanied by an inflammatory response, and it has been shown that IL6-JAK2-STAT3/STAT1 is a key mechanism for effective treatment of IPF, and this treatment is associated with an induced inflammatory response against IL-6 [38]. We examined the levels of IL-6 in the alveolar perfusate and serum of mice, respectively, and showed that compared with BLM-induced mice, CCP significantly reduced their IL-6 expression (Figure 5F and G). The expression of TGF- β 1 in mouse lung tissue was determined by Western blot (Figure 5H and I). The results showed that the expression of TGF- β 1 was significantly increased in the BLM group; Compared with the BLM, the mice in the Nin administration groups showed lower expression levels of TGF- β 1, but not statistically significant; CCP treatment significantly reduced the expression levels of TGF- β 1 in lung tissues. This result suggests that CCP administration alleviates lung fibrosis in mice by reducing the expression level of TGF- β 1.

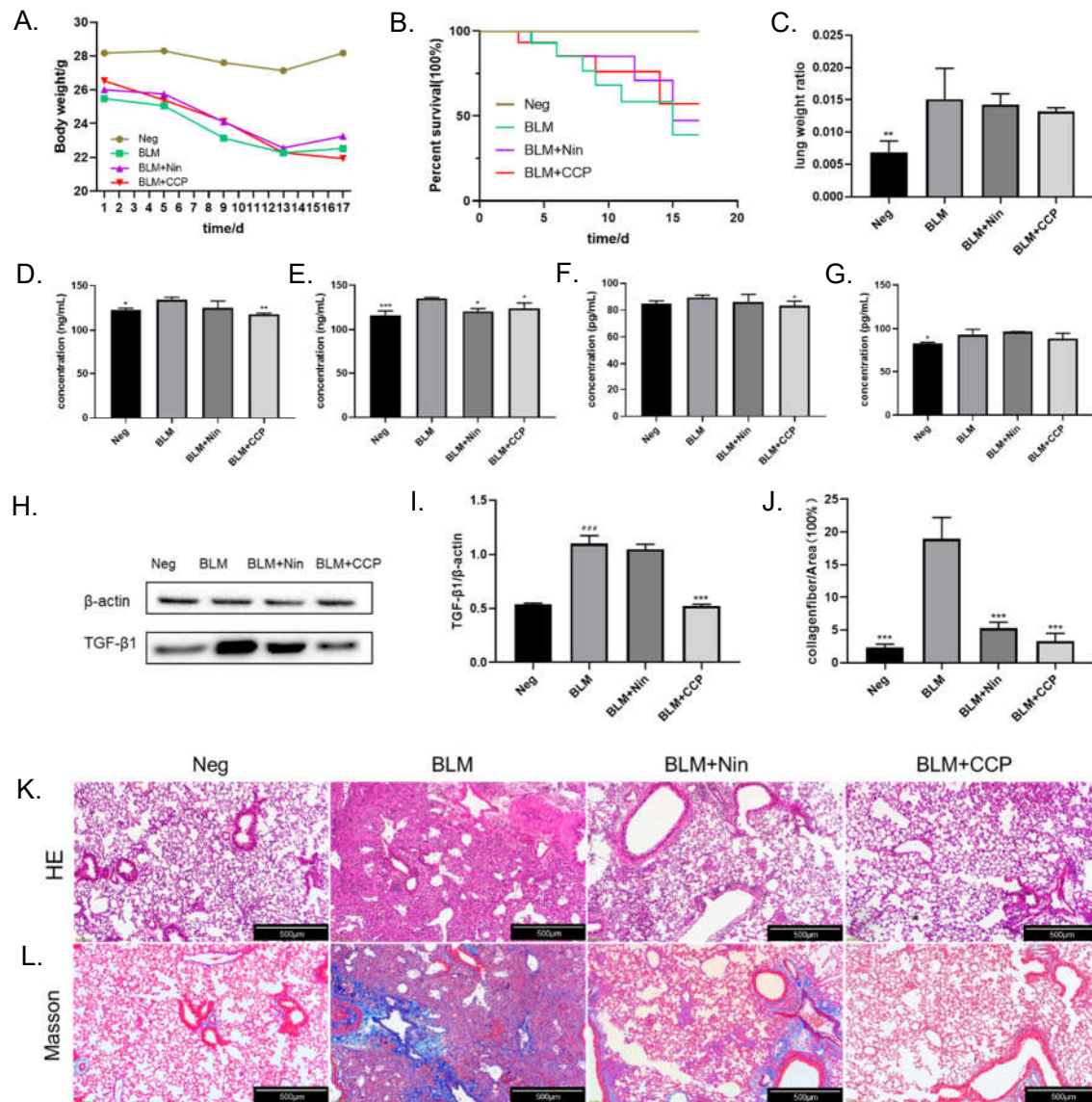


Figure 5. CCP has a palliative effect on bleomycin (BLM)-induced pulmonary fibrosis in mice. (Neg) negative control group, (BLM) BLM (5 mg/kg)-induced group, (BLM+Nin) BLM (5 mg/kg)+Nin (50 mg/Kg)-induced group, and (BLM+CCP) BLM (5 mg/kg)+CCP (200 mg/kg)-induced group. Body weight (A), survival rate (B), (C)lung-to-weight ratio, compared to BLM group: ** $p < 0.01$, concentration of TGF- β 1 in lung flushing fluid (D), concentration of TGF- β 1 in serum (E), concentration of IL-6 in lung flushing fluid (F), concentration of IL-6 in serum (G) were determined. The protein levels of TGF- β 1 from mice treated with BLM, BLM + Nin, BLM + CCP or negative control (Neg) were determined by western blot (H). and analyzed by Image J (I), compared to BLM group: *** $p < 0.001$. Collagen fiber to area ratio in Masson's trichrome staining (J) was quantitatively calculated using Image J. Representative images of HE-stained (K) and Masson's trichrome-stained (L) lung sections from mice were shown. Scale lengths in the diagram represent 500 μ m. Data are shown as the means \pm SEM. * $p < 0.05$, ** $p < 0.01$, *** $p < 0.001$.

To evaluate the histopathological changes of lung tissue, we performed HE staining and Masson staining on mouse lung sections 17 days after BLM injection. The HE staining image is shown in Figure 5K, the negative group showed intact alveolar space structure as well as normal alveolar compartments thickness. Our study found that BLM can cause severe alveolar and interstitial damage accompanied by inflammation, and severe pulmonary fibrotic lesions. After CCP and Nin treatment, the pathological changes of the lung were improved. There were less cell hyperplasia and less damage to alveolar areas and lung structures. The results of Masson staining (Figure 5L)

indicated that BLM injection resulted in excessive deposition of mature collagen in the lungs of mice. The collagen deposition was significantly reduced after CCP and Nin treatment compared with BLM group, but there are still a small amount of collagen found in Nin group. Quantitative analysis of the Masson staining results (Figure 5J) yielded that, compared to the BLM group, Nin and CCP administration group reduced the percentage of collagen by 13.67%, 16.01%, respectively.

4. Conclusions

In this study, we successfully extracted fucoidan (CCP) from *Costaria costata*, which is a sulfated polymer of galactose and fucose. The molecular weight of CCP is about 150 kDa, and the sulfate group content is 18.54%. Our study firstly evaluated the anti-idiopathic fibrosis activity of CCP, and fund CCP exhibited anti-EMT activity in TGF- β 1-induced A549 cells. Its anti-EMT effect was regulated through both the TGF- β /Smad signaling pathway and the PI3K/AKT/mTOR signaling pathway. In addition, CCP exhibited potent anti-pulmonary fibrosis activity *in vivo*, by reducing collagen deposits and down-regulated the expression of TGF- β 1 and IL-6. Therefore, this study proposed a new trehalose gum for the treatment of pulmonary interstitial fibrosis. However, the anti-pulmonary fibrosis mechanism of CCP still needs to be further investigated.

Author Contributions: Sijie Wei performed the experiments and write the manuscript; Wang Jing, Yang Yue, Lihua Geng, and Quanbin Zhang monitor, review, and analyze data; Ning Wu funded and conceived the experiment, and also reviewed the manuscript. All authors have read and agreed to the published version of the manuscript.

Institutional Review Board Statement: All animals were cared for in accordance with the NIH Guide for the Care and Use of Laboratory Animals, and the Experimental Design of this study was approved by the Animal Experimentation Ethics Committee of the Institute of Oceanography, Chinese Academy of Sciences (Approval Code: CTEC-2022-02-01, Approval Date: 7 March 2022).

Conflicts of interest: There are no conflicts to declare.

Funding: This work was supported by the National Key R&D Program of China (2022YFD2401203) and also supported by Nantong Science and technology project (MS12021037).

Nomenclature

Abbreviations	Fullname
CCP	<i>Costaria costata</i> polysaccharide
TGF- β 1	Transforming growth factor- β 1
EMT	Epithelial-mesenchymal transition
COL2A1	Collagen, type II, alpha 1
BLM	Bleomycin
IPF	Idiopathic pulmonary fibrosis
ECM	Extracellular matrix
MMP-1	Matrix Metalloproteinase-1 Promoter
PMP	1-phenyl-3-methyl-5-pyrazolone
DMSO	Dimethyl sulfoxide
MTT	3-(4, 5-dimethylthiazol-2-yl)-2, 5-diphenyltetrazolium bromide
ELISA	Enzyme linked immunosorbent assay
IL-6	Interleukin-6
TPA	Total Phenol Assay

References

- [1] Srour, N., & Thébaud, B. (2015). Mesenchymal stromal cells in animal bleomycin pulmonary fibrosis models: a systematic review. *Stem cells translational medicine*, 4(12), 1500-1510. <https://doi.org/10.5966/sctm.2015-0121>

- [2] Meltzer, E. B., & Noble, P. W. (2008). Idiopathic pulmonary fibrosis. *Orphanet journal of rare diseases*, 3(1), 1-15. <http://www.ijrd.com/content/3/1/8>
- [3] Moon, H. J., Park, K. S., Ku, M. J., Lee, M. S., Jeong, S. H., Imbs, T. I., ... & Lee, Y. H. (2009). Effect of *Costaria costata* fucoidan on expression of matrix metalloproteinase-1 promoter, mRNA, and protein. *Journal of Natural Products*, 72(10), 1731-1734. <https://doi.org/10.1021/np800797v>
- [4] Wang, Q., Song, Y., He, Y., Ren, D., Kow, F., Qiao, Z., ... & Yu, X. (2014). Structural characterisation of algae *Costaria costata* fucoidan and its effects on CCl₄-induced liver injury. *Carbohydrate polymers*, 107, 247-254. <https://doi.org/10.1016/j.carbpol.2014.02.071>
- [5] McLean, J. H. (1962). Sublittoral ecology of kelp beds of the open coast area near Carmel, California. *The Biological Bulletin*, 122(1), 95-114. <https://www.journals.uchicago.edu/toc/bbl/1962/122/1>
- [6] Van Weelden, G., Bobiński, M., Okła, K., Van Weelden, W. J., Romano, A., & Pijnenborg, J. M. (2019). Fucoidan structure and activity in relation to anti-cancer mechanisms. *Marine drugs*, 17(1), 32. <https://doi.org/10.3390/md17010032>
- [7] Li, B., Lu, F., Wei, X., & Zhao, R. (2008). Fucoidan: structure and bioactivity. *Molecules*, 13(8), 1671-1695. <https://doi.org/10.3390/molecules13081671>
- [8] January, G. G., Naidoo, R. K., Kirby-McCullough, B., & Bauer, R. (2019). Assessing methodologies for fucoidan extraction from South African brown algae. *Algal Research*, 40, 101517. <https://doi.org/10.1016/j.algal.2019.101517>
- [9] Li, S. S., Wang, Q. K., He, Y. H., Ren, D. D., & Zhang, Z. Y. (2013). The extraction of serum lipids reducing function of fucoidan from seaweed *Costaria costata*. *J Dalian Ocean Univ*, 28(1), 93-98.
- [10] Monsur, H. A., Jaswir, I., Simsek, S., Amid, A., Alam, Z., & Tawakalit, A. H. (2014). Cytotoxicity and inhibition of nitric oxide syntheses in LPS induced macrophage by water soluble fractions of brown seaweed. *Food Hydrocolloids*, 42, 269-274. <https://doi.org/10.1016/j.foodhyd.2014.02.021>
- [11] Jin, W., Wang, J., Jiang, H., Song, N., Zhang, W., & Zhang, Q. (2013)a. The neuroprotective activities of heteropolysaccharides extracted from *Saccharina japonica*. *Carbohydrate polymers*, 97(1), 116-120. <https://doi.org/10.1016/j.carbpol.2013.04.055>
- [12] Bitter, T. (1962). A modified uronic acid carbazole reaction. *Anal. Biochem.*, 4, 330-334.
- [13] DuBois, M., Gilles, K. A., Hamilton, J. K., Rebers, P. T., & Smith, F. (1956). Colorimetric method for determination of sugars and related substances. *Analytical chemistry*, 28(3), 350-356.
- [14] Gibbons, M. N. (1955). The determination of methylpentoses. *Analyst*, 80(949), 268-276.
- [15] Zhang, J., Zhang, Q., Wang, J., Shi, X., & Zhang, Z. (2009). Analysis of the monosaccharide composition of fucoidan by precolumn derivation HPLC. *Chinese Journal of Oceanology and Limnology*, 27(3), 578-582. <https://doi.org/10.1007/s00343-009-9205-0>
- [16] Davoren, M., Herzog, E., Casey, A., Cottineau, B., Chambers, G., Byrne, H. J., & Lyng, F. M. (2007). *In vitro* toxicity evaluation of single walled carbon nanotubes on human A549 lung cells. *Toxicology in vitro*, 21(3), 438-448. <https://doi.org/10.1016/j.tiv.2006.10.007>
- [17] Yang, F., Xiong, H., Duan, L., Li, Q., Li, X., & Zhou, Y. (2019). MiR-1246 promotes metastasis and invasion of A549 cells by targeting GSK-3 β -mediated Wnt/ β -catenin pathway. *Cancer Res Treat*, 51(4), 1420-1429. <https://doi.org/10.4143/crt.2018.638>
- [18] Ortiz, J., Romero, N., Robert, P., Araya, J., Lopez-Hernández, J., Bozzo, C., ... & Rios, A. (2006). Dietary fiber, amino acid, fatty acid and tocopherol contents of the edible seaweeds *Ulva lactuca* and *Durvillaea antarctica*. *Food chemistry*, 99(1), 98-104. <https://doi.org/10.1016/j.foodchem.2005.07.027>
- [19] Aguilera-Morales, M., Casas-Valdez, M., Carrillo-Dominguez, S., González-Acosta, B., & Pérez-Gil, F. (2005). Chemical composition and microbiological assays of marine algae *Enteromorpha* spp. as a potential food source. *Journal of food composition and analysis*, 18(1), 79-88. <https://doi.org/10.1016/j.jfca.2003.12.012>
- [20] Zhang, R., Zhang, X., Tang, Y., & Mao, J. (2020). Composition, isolation, purification and biological activities of *Sargassum fusiforme* polysaccharides: A review. *Carbohydrate polymers*, 228, 115381. <https://doi.org/10.1016/j.carbpol.2019.115381>
- [21] Jin, W., Zhang, Q., Wang, J., & Zhang, W. (2013)b. A comparative study of the anticoagulant activities of eleven fucoidans. *Carbohydrate polymers*, 91(1), 1-6. <https://doi.org/10.1016/j.carbpol.2012.07.067>
- [22] Ale, M. T., Mikkelsen, J. D., & Meyer, A. S. (2012). Designed optimization of a single-step extraction of fucose-containing sulfated polysaccharides from *Sargassum* sp. *Journal of applied phycology*, 24, 715-723. <https://doi.org/10.1007/s10811-011-9690-3>
- [23] Li, R., Zhou, Q. L., Chen, S. T., Tai, M. R., Cai, H. Y., Ding, R., ... & Zhong, S. Y. (2023) Chemical Characterization and Immunomodulatory Activity of Fucoidan from *Sargassum hemiphyllum*. *Marine drugs* 2023,21, 18. <https://doi.org/10.3390/md21010018>
- [24] Baek, A. R., Lee, J. M., Seo, H. J., Park, J. S., Lee, J. H., Park, S. W., ... & Park, C. S. (2016). Apolipoprotein A1 Inhibits TGF- β 1-Induced Epithelial-to-Mesenchymal Transition of Alveolar Epithelial Cells. *Tuberculosis and respiratory diseases*, 79(3), 143-152. <https://doi.org/10.4046/trd.2016.79.3.143>

- [25] Han, M. L., Zhao, Y. F., Tan, C. H., Xiong, Y. J., Wang, W. J., Wu, F., ... & Liang, Z. Q. (2016). Cathepsin L upregulation-induced EMT phenotype is associated with the acquisition of cisplatin or paclitaxel resistance in A549 cells. *Acta Pharmacologica Sinica*, 37(12), 1606-1622. <https://doi.org/10.1038/aps.2016.93>
- [26] Yuan, W., Wei, F., Ouyang, H., Ren, X., Hang, J., Mo, X., & Liu, Z. (2021). CMTM3 suppresses chordoma progress through EGFR/STAT3 regulated EMT and TP53 signaling pathway. *Cancer Cell International*, 21, 1-18. <https://doi.org/10.1186/s12935-021-02159-5>
- [27] Liu, S., Ye, D., Xu, D., Liao, Y., Zhang, L., Liu, L., ... & Zhang, Z. (2016). Autocrine epiregulin activates EGFR pathway for lung metastasis via EMT in salivary adenoid cystic carcinoma. *Oncotarget*, 7(18), 25251. <https://doi.org/10.18632/oncotarget.7940>
- [28] Liu, L., Sun, Q., Davis, F., Mao, J., Zhao, H., & Ma, D. (2022). Epithelial-mesenchymal transition in organ fibrosis development: current understanding and treatment strategies. *Burns & Trauma*, 10. <https://doi.org/10.1093/burnst/tkac011>
- [29] Chen, L., Yang, T., Lu, D. W., Zhao, H., Feng, Y. L., Chen, H., ... & Zhao, Y. Y. (2018). Central role of dysregulation of TGF- β /Smad in CKD progression and potential targets of its treatment. *Biomedicine & Pharmacotherapy*, 101, 670-681. <https://doi.org/10.1016/j.biopha.2018.02.090>
- [30] Hu, H. H., Chen, D. Q., Wang, Y. N., Feng, Y. L., Cao, G., Vaziri, N. D., & Zhao, Y. Y. (2018). New insights into TGF- β /Smad signaling in tissue fibrosis. *Chemico-biological interactions*, 292, 76-83. <https://doi.org/10.1016/j.cbi.2018.07.008>
- [31] Yang, F., Huang, X. R., Chung, A. C., Hou, C. C., Lai, K. N., & Lan, H. Y. (2010). Essential role for Smad3 in angiotensin II-induced tubular epithelial-mesenchymal transition. *The Journal of pathology*, 221(4), 390-401. <https://doi.org/10.1002/path.2721>
- [32] Naber, H. P., Drabsch, Y., Snaar-Jagalska, B. E., ten Dijke, P., & van Laar, T. (2013). Snail and Slug, key regulators of TGF- β -induced EMT, are sufficient for the induction of single-cell invasion. *Biochemical and biophysical research communications*, 435(1), 58-63. <https://doi.org/10.1016/j.bbrc.2013.04.037>
- [33] Haslehurst, A. M., Koti, M., Dharsee, M., Nuin, P., Evans, K., Geraci, J., ... & Feilolter, H. (2012). EMT transcription factors snail and slug directly contribute to cisplatin resistance in ovarian cancer. *BMC cancer*, 12, 1-10. <https://doi.org/10.1186/1471-2407-12-91>
- [34] Larue, L., & Bellacosa, A. (2005). Epithelial-mesenchymal transition in development and cancer: role of phosphatidylinositol 3' kinase/AKT pathways. *Oncogene*, 24(50), 7443-7454. <https://doi.org/10.1038/sj.onc.1209091>
- [35] Wu, N., Li, Z., Wang, J., Geng, L., Yue, Y., Deng, Z., ... & Zhang, Q. (2021). Low molecular weight fucoidan attenuating pulmonary fibrosis by relieving inflammatory reaction and progression of epithelial-mesenchymal transition. *Carbohydrate Polymers*, 273, 118567. <https://doi.org/10.1016/j.carbpol.2021.118567>
- [36] Moeller, A., Ask, K., Warburton, D., Gaudie, J., & Kolb, M. (2008). The bleomycin animal model: a useful tool to investigate treatment options for idiopathic pulmonary fibrosis?. *The international journal of biochemistry & cell biology*, 40(3), 362-382. <https://doi.org/10.1016/j.biocel.2007.08.011>
- [37] Liu, T., De Los Santos, F. G., & Phan, S. H. (2017). The bleomycin model of pulmonary fibrosis. *Fibrosis: Methods and Protocols*, 27-42.
- [38] Xue, Z., Zhao, F., Sang, X., Qiao, Y., Shao, R., Wang, Y., ... & Yang, J. (2021). Combination therapy of tanshinone IIA and puerarin for pulmonary fibrosis via targeting IL6-JAK2-STAT3/STAT1 signaling pathways. *Phytotherapy Research*, 35(10), 5883-5898. <https://doi.org/10.1002/ptr.7253>